On the Mechanism of Electrohydrodynamic Convection in Thin-Layer Electrolytic Cells

Marek Orlik,† Karl Doblhofer,* and Gerhard Ertl

Fritz-Haber-Institut der Max-Planck-Gesellschaft, Faradayweg 4-6, D-14195 Berlin, Germany

Received: February 3, 1998; In Final Form: May 18, 1998

In thin-layer cells the electrochemical current flow can give rise to electrohydrodynamic (EHD) convection of the electrolyte. If combined with a system exhibiting electrochemiluminescence, these convective patterns become directly visible. Following previous experimental work, in this paper a theoretical model is presented and analyzed. It comprises numerical simulation of diffusion and migration of electroactive species (rubrene molecules and ions) and of electroinactive ions of supporting electrolyte across the 100 μm wide gap between the electrodes. The driving force for convection across the thin layer results from the product of the local uncompensated charge (carried by the liquid) and the local electric field. Characteristic concentration profiles of the species involved are presented, and the role of varying mobilities of the ions of the supporting electrolyte, as well as the additional complexity of the local electric field distribution, resulting from recombination of the rubrene ions is analyzed. Finally, comparison with experimental data is sketched.

1. Introduction

Electrolysis of rubrene dissolved in 1,2-dimethoxyethane (1,2-DME) in a thin-layer cell leads to the formation of electrohydrodynamic (EHD) convective patterns of electrochemiluminescence (ECL), which sometimes closely resemble the well-known Bénard patterns.[1−3] These effects were first described by Schaper, Schnedler, and Köstlin[4−7] several years ago. In a previous paper[8] we described an appropriate experimental setup, showed typical patterns, and proposed a qualitative mechanism for the driving force for electroconvection and for the processes leading to the flow of current. For illustration, Figure 1 shows another example of a luminescent pattern formed in this way by using the described experimental arrangement.

In the present paper we describe a quantitative model that is then used for numerical simulation of the state of the system at the time after application of the cell voltage. The emphasis will be on the quantitative description of the driving forces for convection of the electrolyte.

2. The Model

The mechanism for pattern formation proposed previously[8] is briefly outlined by Figure 2: Molecules of rubrene (5,6,11, 12-tetraphenylnaphthacene) undergo fast and reversible electroreduction and -oxidation, respectively, at the respective electrodes. The produced R^+ and R^- radical ions diffuse and migrate toward the respective opposite electrode. Where they meet, recombination leads to formation of excited molecules that are emitting light: $R^+ + R^- \rightarrow R + R^* \rightarrow 2R + h\nu$. The locations of luminescence are determined by the convective flow of cations to the anode where the product of the concentrations of cations with that of the electrochemically formed anions becomes highest, and analogous considerations hold for the region near the cathode. The driving force for convection is determined by the space charge interacting with the electric field.

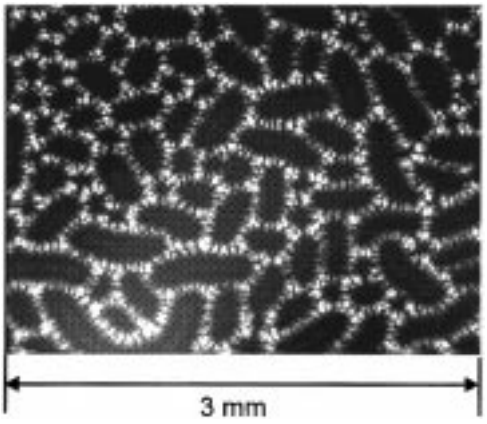

Figure 1. Example convective structure appearing in the thin-layer cell as a result of the electrolysis of saturated ($\sim 4 \times 10^{-3}$ mol dm^{-3}) solution of rubrene in 1,2-dimethoxyethane, in the presence of 1.2×10^{-5} mol dm^{-3} tetrabutylammonium hexafluorophosphate as a supporting electrolyte. The convective flows are visualized by the spatial distribution of electrochemiluminescence occurring in the places of recombination of rubrene radical cations and anions, close to the cathode surface. In the centers of some convective cells also traces of anodic luminescence become visible. A voltage of 4 V was applied between the platinum cathode and the anode−glass plate, covered by conducting ITO (indium−tin-oxide) transparent layer. Interelectrode distance $d =$ 90 μm.

In this connection the presence of ions from the supporting electrolyte (tetrabutylammonium hexafluorophosphate = $TBA^+ + HFP^-$) is decisive.

The literature contains various treatments of transport processes involving both diffusion and migration, for example, for conditions modeling semiconductor electrodes[9] or for chronoamperometry in the presence of low concentration of supporting electrolyte.[10] These approaches were adopted to the present problem of a thin-layer system with local excess charge as the starting point for the model. It describes the flow of faradaic current I through the thin-layer cell for the case that the concentration of supporting electrolyte is much (i.e., 100−500 times) lower than the maximum concentration (4×10^{-3} mol dm^{-3}) of the electroactive species rubrene. This means that

* Corresponding author. Fax, (+030) 8413-3101; e-mail, doblhofer@fhi-berlin.mpg.de.

† Permanent address: The University of Warsaw, Department of Chemistry, ul. Pasteura 1, 02-093 Warsaw, Poland.

S1089-5647(98)00995-X CCC: $15.00
Published on Web 07/25/1998

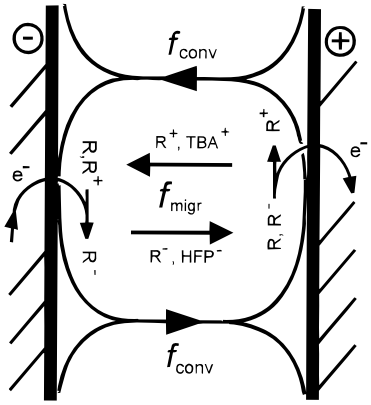

Figure 2. Scheme for the processes occurring within a single convective roll. The electrochemical reactions of rubrene at both electrodes are accompanied by convection (f_{conv}) and migration (f_{migr}) of ions of rubrene and the supporting electrolyte. For simplicification, diffusion fluxes are not indicated. Recombination between R^+ and R^- in the front of both electrodes leads to chemiluminescence.[8]

the magnitude of the current is controlled by a relatively high ohmic resistance R of the solution, and thus only a *small fraction* of rubrene can be electrolyzed at both electrodes. This resistance varies continuously with the actual composition of the thin layer electrolyte. Hence, contributions by all charge carriers, ions of supporting electrolyte as well as rubrene ions created at the electrodes, are essential for the current.

The actual distribution of the electric field ($\mathbf{E} = -\nabla\varphi$) in the solution is associated with the magnitude of charge flow injected at the electrodes and transported through the solution by both diffusion and migration. The local density of uncompensated charge q_{ex} is coupled with the local divergence of the electric field (div $\mathbf{E} = -\nabla^2\varphi$) through Poisson's equation:

$$q_{ex}(x, y, z, t) = -\epsilon\epsilon_0\nabla^2\varphi \tag{1}$$

The calculations reported in the following were conducted for the time shortly after the voltage had been applied. For this period the assumption was made that the solution remained still quiescent. Then the electrochemical processes can be approximated by a one-dimensional model for the spatial coordinate x oriented across the gap between the two electrodes, along a normal to the electrode surfaces, and Poisson's equation reduces to

$$q_{ex}(x, t) = -\epsilon\epsilon_0\frac{\partial^2\varphi}{\partial x^2} \tag{2}$$

The electroconvection is caused by the force of a density F_{ex} resulting from the interaction of the electric field with volume elements of fluid, carrying an excess charge density q_{ex}:

$$|\mathbf{F}_{ex}| = F_{ex} = -q_{ex}\left(\frac{\partial\varphi}{\partial x}\right) = \epsilon\epsilon_0\left(\frac{\partial^2\varphi}{\partial x^2}\right)\left(\frac{\partial\varphi}{\partial x}\right) \tag{3}$$

Figure 3 shows schematically the distribution of the electric potential in the thin-layer cell, including potential drops in the electrical double layers at both electrodes. The shaded area corresponds to the x_{tr} distance over which transport phenomena associated with the electric field develop, caused by the flow of current I through the solution with a resistance R

$$IR = \int_{x_{dl}^c}^{d-x_{dl}^a}\left(\frac{\partial\varphi}{\partial x}\right)\mathrm{d}x \tag{4}$$

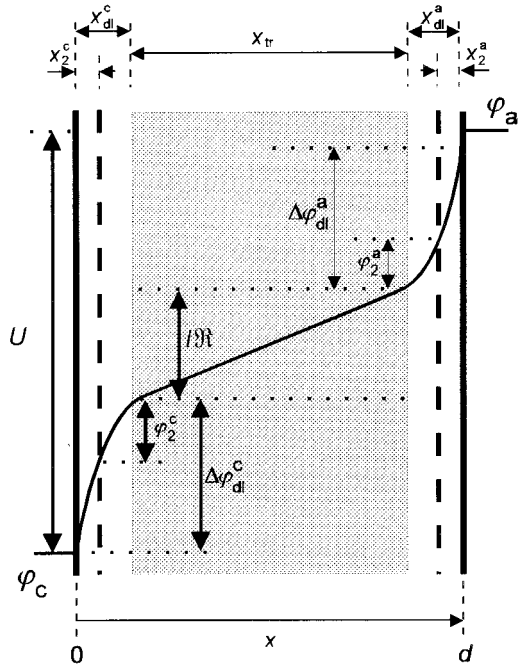

Figure 3. Schematic sketch of potential distribution across the interelectrode space (d) of the thin-layer two-electrode cell. $U = \varphi_a - \varphi_c$ = total voltage applied from external source; φ_2^c, φ_2^a, cathodic and anodic potentials at the outer Helmholtz planes, separated from the respective electrode surfaces by distances x_2^c and x_2^a respectively. x_{dl}^c, $\Delta\varphi_{dl}^c$, x_{dl}^a, $\Delta\varphi_{dl}^a$, the extent and the total potential drop in the cathodic and anodic double layer, respectively; I, electric current flowing through the cell; R ohmic resistance of the solution. The coupled diffusion and migration phenomena and associated electric field distribution were modeled for the region $x_{tr} \cong d$ shown as shaded area.

Our model comprises a simplification insofar as the distance x_{tr}, responsible for conduction of the current by diffusion and migration, is approximated by the *entire* interelectrode distance d. This assumption is well-justified, as a simple calculation shows: for typical concentrations of 1:1 supporting electrolyte between 5×10^{-6} and 2×10^{-5} mol dm^{-3}, the extension of the diffuse parts of double layers, x_{dl}, estimated to be 1.5 times the Debye length $\kappa^{-1} = [\epsilon\epsilon_0 RT/(2F^2c^0)]^{1/2}$ with $\epsilon = 7.2$ for 1,2-DME,[11] results to be in the range between 60 and 30 nm. Even for the smallest interelectrode distance of 50 μm, this is only of the order of 0.1% of d, so that indeed $x_{tr} \cong d$ (cf. Figure 3).

The simulation of double layers would mean a significant but unnecessary complication of the model. Therefore, the starting point for modeling the driving force for convection corresponds to the real situation when double layers at both electrodes are already formed to the extent necessary for the electrode processes of rubrene to begin. Rough calculations show that the time constant of the thin-layer ($d = 100$ μm) electrolytic system, which consists of serially connected two capacitors and the solution resistance (determined by the presence of 1×10^{-5} mol dm^{-3} 1:1 ionic salt) remains within 16−40 ms. The zero point of the time scale used for the following simulations is thus 16−40 ms after the time at which the potential was applied to the cell.

Furthermore, since the total concentration of electrolyte was relatively low (10^{-5} mol dm^{-3}), it was assumed that thermodynamical activities of all ions can be well-estimated by their concentrations and that diffusion coefficients of all species are independent of the local concentration.

The individual electrode potentials were calculated in the following way. First, we assume that: (i) the points of zero charge of both electrodes are at $E = 0$ V, i.e., $U = \varphi_a - \varphi_c$ (cf.

TABLE 1: Model Parameters for Simulation of Diffusion and Migration Transport in the Thin-Layer Cell, in Which Rubrene Is Electrolyzed in the Presence of a Low Amount of Supporting Electrolyte[a]

simulation parameter	symbol	value
temperature	T	298.15 K
Electrode surface area	A	1 cm^2
interelectrode distance	d	100 μm
external voltage	U	5 V
dielectric constant of the solvent (1,2-DME)	ϵ	7.2
bulk rubrene (R) concentration	c_R^0	4×10^{-3} mol dm^{-3}
bulk supporting electrolyte (salt) concentration	c_s^0	1×10^{-5} mol dm^{-3}
formal potential of R/R$^-$	E_1^0	-1.13 V
formal potential of R/R$^+$	E_2^0	$+1.37$ V
charge of cations of rubrene	z_{R^+}	$+1$
charge of anions of rubrene	z_{R^-}	-1
charge of cations of the salt	z_{Cat}	$+1$
charge of anions of the salt	z_{An}	-1
rate constant of recombination of rubrene ions	k_r	1×10^{10} dm^3 mol^{-1} s^{-1}
diffusion coefficient of R	D_R	6.2×10^{-6} cm^2 s^{-1}
diffusion coefficient of R$^+$	D_{R^+}	6.2×10^{-6} cm^2 s^{-1}
diffusion coefficient of R$^-$	D_{R^-}	6.2×10^{-6} cm^2 s^{-1}
diffusion coefficient of cation of supporting electrolyte	D_{Cat}	6.2×10^{-6} cm^2 s^{-1}
diffusion coefficient of anion of supporting electrolyte	D_{An}	(a) 6.2×10^{-6} cm^2 s^{-1} (b) 2.8×10^{-5} cm^2 s^{-1}

[a] Two series of simulations were performed, for different values of D_{An} (cf. last row).

Figure 3); (ii) there are no differences in the structure of double layers (cf. Figure 3); (iii) the potential drop in the ITO layer of the transparent electrode is negligible, and thus the ohmic potential drop is due exclusively to a solution resistance R. Furthermore, since a reference electrode is not used in our (two-electrode) experimental system,[8] we define, for our convenience, an electrode potential scale involving the arithmetic mean of the formal potentials of R$^-$/R (E_1^0) and R$^+$/R (E_2^0) couples. Then, owing to assumed symmetrical charge injection at both electrodes,[8] their potentials differ from the $(E_1^0 + E_2^0)/2$ value equally in the cathodic and anodic direction, for the half of the total voltage U, diminished by total ohmic drop (I) in the solution:

$$E_{cath} = \left[\frac{E_1^0 + E_2^0}{2}\right] - \left[\frac{|U| - |I|R}{2}\right] \tag{5}$$

$$E_{anod} = \left[\frac{E_1^0 + E_2^0}{2}\right] + \left[\frac{|U| - |I|R}{2}\right] \tag{6}$$

For our calculations we used literature[16] data of E_1^0 and E_2^0 determined with respect to W wire as a reference electrode (cf. Table 1).

R, a total resistance of the solution between the two electrodes, is defined by

$$R = \frac{1}{A}\int_0^d \frac{dx}{\kappa(x)} = \frac{RT}{AF^2}\int_0^d \frac{dx}{\sum_s z_s^2 D_s c_s(x,t)} \tag{7}$$

Here, A is the surface area of the electrode, $\kappa(x)$ is the conductivity, and the summation is performed over all charged species s with ionic charges z_s, diffusion coefficient D_s, and concentration $c_s(x)$.

As outlined above, the produced R$^+$ and R$^-$ ions migrate and diffuse toward the respective opposite electrode, and when they meet, they recombine with a rate constant k_r. A small number eventually reaching the opposite electrode is recharged there. The electric current I can be related to the fluxes f_s of the respective species in the following way:

$$I(t) = FA[f_R(0,t) + 2f_{R^+}(0,t)] = -FA[f_{R^-}(0,t) - f_{R^+}(0,t)] \tag{8}$$

$$I(t) = -FA[f_R(d,t) + 2f_{R^-}(d,t)] = FA[f_{R^+}(d,t) - f_{R^-}(d,t)] \tag{9}$$

Thereby the net fluxes of all electroactive substances at both electrodes ($x = 0$ for cathode and $x = d$ for anode) are equal to zero (no rubrene adsorption on the surfaces):

$$f_R(0,t) + f_{R^+}(0,t) + f_{R^-}(0,t) = 0 \tag{10}$$

$$f_R(d,t) + f_{R^+}(d,t) + f_{R^-}(d,t) = 0 \tag{11}$$

The surface ($x = 0$, $x =$ d) and bulk ($0 < x < d$) fluxes are given by the following general expression, involving migration of charged particles in the electric field

$$f_s(x,t) = -D_s\left(\frac{\partial c_s}{\partial x}\right) + z_s\frac{F}{RT}D_s c_s \mathbf{E}(x,t) \tag{12}$$

where $\mathbf{E}(x,t) = -\partial\varphi(x,t)/\partial x$ is the local electric field, and ionic charges, $z_{R^+} = z_{Cat} = +1$, $z_{R^-} = z_{An} = -1$, and $z_R = 0$. One should note that for a nonelectroactive supporting electrolyte the individual *surface* fluxes of the ions (Cat, An) are equal to zero.

The surface concentrations of all rubrene species obey the corresponding Nernst equations:

$$E_{cath} = E_1^0 + \frac{RT}{F}\ln\frac{c_R(0,t)}{c_{R^-}(0,t)} = E_2^0 + \frac{RT}{F}\ln\frac{c_{R^+}(0,t)}{c_R(0,t)} \tag{13}$$

$$E_{anod} = E_2^0 + \frac{RT}{F}\ln\frac{c_{R^+}(d,t)}{c_R(d,t)} = E_1^0 + \frac{RT}{F}\ln\frac{c_R(d,t)}{c_{R^-}(d,t)} \tag{14}$$

The current I is transferred through the solution by all charge carriers, according to the relationship

$$I(t) = FA\sum_s z_s f_s(x,t) = -FA\left[\sum_s z_s D_s\frac{\partial c_s}{\partial x} - \frac{F}{RT}\mathbf{E}(x,t)\sum_s z_s^2 D_s c_s\right] \tag{15}$$

This yields the equation for the local electric field

$$-\mathbf{E}(x,t) \equiv \frac{\partial\varphi}{\partial x} = \frac{-RT}{F^2\sum_s z_s^2 D_s c_s}\left[\frac{I(t)}{A} + F\sum_s z_s D_s\frac{\partial c_s}{\partial x}\right] \tag{16}$$

The temporal changes of the local concentration of every species s are given by the continuity equation

$$\frac{\partial c_s}{\partial t} = -\frac{\partial f_s}{\partial x} + T_{chem,s} \tag{17}$$

where $T_{chem,s}$ describes the contribution from the chemical recombination of rubrene ions

$$T_{\mathrm{chem,s}} = \begin{cases} -k_r c_{R^+} c_{R^-} & s = R^+, R^- \\ +2k_r c_{R^+} c_{R^-} & s = R^0 \\ 0 & s = \mathrm{Cat, An} \end{cases} \quad (18)$$

Finally, the local uncompensated charge is introduced, which is responsible for the driving force of electroconvection and enters Poisson's eq 2

$$\sum_s z_s c_s(x, t) = \frac{q_{ex}(x, t)}{F} \quad (19)$$

3. Computational Procedure

The differential equations describing the transport processes were integrated by using the explicit finite differences method.[12−14] The scheme for discretization of the interelectrode distance d into M intervals with thickness Δx is sketched in Figure 4. The local concentrations and fluxes of all species and the local electric fields are denoted by $c(i, l)$, $f(i, l)$, and $\mathbf{E}(i, l)$, respectively, whereby the index $i = 0, ..., M$ corresponds to the spatial coordinate ($=i\Delta x$), and index l the temporal coordinate ($=l\Delta t$).

According to the geometrical positions of concentrations and electric fields points, the fluxes $f_s(i, l)$ ($i = 0, ..., M-1$, $l = 1, ..., N$) are expressed by the following difference formula:

$$f_s(i, l) = -D_s \frac{c_s(i+1, l) - c_s(i, l)}{\Delta x} + z_s \frac{F}{RT} D_s \mathbf{E}(i, l) \left(\frac{c_s(i+1, l) + c_s(i, l)}{2} \right) \quad (20)$$

where

$$-\mathbf{E}(i, l) \equiv \left[\frac{\Delta\varphi}{\Delta x}\right]_{i,l} = \frac{-2RT}{F^2 \sum_s z_s^2 D_s [c_s(i+1, l) + c_s(i, l)]} \left[\frac{I(l)}{A} + F \sum_s z_s D_s \frac{c_s(i+1, l) - c_s(i, l)}{\Delta x} \right] \quad (21)$$

The computational scheme, performed for a constant external voltage U, involved the following main steps, for every time interval t:

(i) Calculation of the actual ohmic resistance $R(l)$ of the solution

$$R(l) = \frac{RT\Delta x}{AF^2} \sum_{i=1}^{M} \frac{1}{\sum_s z_s^2 D_s \frac{[c_s(i-1, l) + c_s(i, l)]}{2}} \quad (22)$$

This was achieved by the numerical integration of eq 7 using the trapezoidal rule.

(ii) Calculation of the faradaic current, according to eqs 8 and 9, which transform into

$$I(l) = FA[f_R(0, l) + 2f_{R^+}(0, l)] = -FA[f_{R^-}(0, l) - f_{R^+}(0, l)] \quad (23)$$

$$I(l) = -FA[f_R(M-1, l) + 2f_{R^-}(M-1, l)] = FA[f_{R^+}(M-1, l) - f_{R^-}(M-1, l)] \quad (24)$$

Thereby, the surface concentrations of rubrene species, necessary for calculations of surface fluxes $f(0, l)$ and $f(M-1, l)$, were found from combination of difference form of eqs 10−12 with eqs 13 and 14.

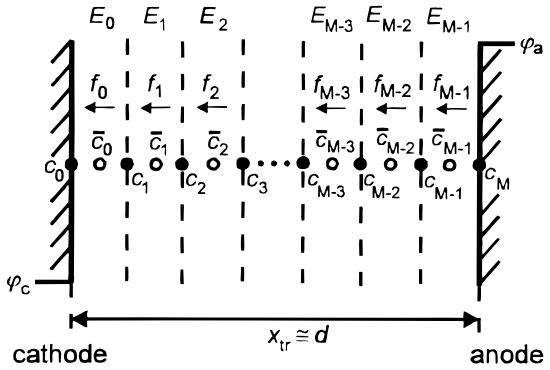

Figure 4. Scheme of discretization of the total interelectrode space (d) into M intervals $\Delta x = d/M$; c_0 and c_M, surface concentrations of a given species; c_i, $i = 1, ..., M-1$, bulk concentrations calculated at the distances $i\Delta x$; $\bar{c}_i$, $i = 0, ..., M-1$ average concentrations; f_i, $i = 0, ..., M-1$, coupled diffusion and migration fluxes; $\mathbf{E}_i$, local electric fields.

Because of the existence of ohmic drops (cf. eqs 5, 6), the current $I(l)$ was not given explicitly but had to be extracted from eqs 23 and 24 numerically as a root of these nonlinear equations, by Müller's procedure (bisection followed by inverse parabolic interpolation[15]).

(iii) Calculation of the surface concentrations of ions of supporting electrolyte from the following relationships of difference expressions of eq 12

$$f_{Cat}(0, l) + f_{An}(0, l) = 0 \quad (25)$$

$$f_{Cat}(M-1, l) + f_{An}(M-1, l) = 0 \quad (26)$$

combined with Poisson's eq 19 for surface ($i = 0$, $i = M$) uncompensated charges. These charges were estimated from the divergence of the electric field $\mathbf{E}$, calculated for ionic concentration distribution at the respective electrode surface ($x = 0$, $x = d$) and at the distances ($\Delta x/2$, $d - (\Delta x/2)$) away from this surface.

(iv) Calculation of the new spatial distribution of the electric field ($\mathbf{E}(i, l)$, $i = 0, ..., M-1$), corresponding to the actual current $I(l)$ (eq 21).

(v) Calculation of the spatial distribution of the driving force for convection, per volume element

$$F_{ex}(i, l) = q_{ex}(i, l) \frac{\mathbf{E}(i, l) + \mathbf{E}(i-1, l)}{2} \quad (27)$$

where

$$q_{ex}(i, l) = \epsilon\epsilon_0 \frac{\mathbf{E}(i, l) - \mathbf{E}(i-1, l)}{\Delta x} \quad (28)$$

(vi) Calculation of the local ($i\Delta x$, $i = 1, ..., M-1$) temporal changes of concentrations of all species in the solution, due to diffusion and migration transports (d-m), as well as due to chemical recombination reactions (chem) for rubrene, leading to new concentrations $c_S(i, l+1)$ at the time step $(l+1)\Delta t$

$$[c_s(i, l+1)]_{d-m} = c_s(i, l) + \frac{\Delta t}{\Delta x}[f_s(i-1, l) - f_s(i, l)] \quad (29)$$

$$c_s(i, l+1) = [c_s(i, l+1)]_{d-m} + (\Delta t) T_{\mathrm{chem,s}}(i, l) \quad (30)$$

where

$$T_{\text{chem,s}}(i, l) =$$

$$\begin{cases} -k_r[c_{R^+}(i, l+1)]_{d-m}[c_{R^-}(i, l+1)]_{d-m} & s = R^+, R^- \\ +2k_r[c_{R^+}(i, l+1)]_{d-m}[c_{R^-}(i, l+1)]_{d-m} & s = R^0 \\ 0 & s = \text{Cat, An} \end{cases} \quad (31)$$

(vii) Adjustment of the highest concentration of the ionic species in every spatial cell ($i\Delta x$, $i = 1, ..., M - 1$) to a value satisfying Poisson's equation

$$z_{\text{Cat}}c_{\text{Cat}}(i, l+1) + z_{R^+}c_{R^+}(i, l+1) + z_{\text{An}}c_{\text{An}}(i, l+1) + z_{R^-}c_{R^-}(i, l+1) = \frac{q_{\text{ex}}(i, l)}{F} \quad (32)$$

This correction is of the order of only 10^{-3}% at early stages of the simulation and quickly decreases to about 10^{-7}%. It practically did not change the current and the electric field distribution but only improved the local balance of concentration of ions, distorted mainly due to limited numerical accuracy of the finite differences method.

(viii) Changing the temporal variable by Δt and return to step i, thus progressing in time; in light of points vi and vii, the final local concentrations at time $(l + 1)\Delta t$ were determined both by the concentration distribution ($\partial c_S/\partial x$) and the electric potential distribution ($\partial\varphi/\partial x$, $\partial^2\varphi/\partial x^2$), at the *preceding* time $l\Delta t$.

The calculations were performed with the set of parameters listed in Table 1. The data for the formal potentials of rubrene redox couples were estimated from cyclic voltammograms of rubrene in 1,2-DME recorded with a Pt electrode in the presence of the supporting electrolyte TBA-HFP (cf. Figure 2 in ref 16), by using a W wire as a quasi-reference electrode (about −0.1 V vs aqueous SCE[16]). The diffusion coefficients were assessed already in our previous paper.[8] The high value for the rate constant k_r for rubrene radical recombination means that this reaction is practically diffusion-controlled.

For all simulations the same set of parameters was taken with the exception of the diffusion coefficient D_{An} for the anions of supporting electrolyte, for which two values were taken: one identical with diffusion coefficients of all the other species, and another one, larger by a factor of 4.5, representing the properties of the supporting electrolyte TBA-HFP, used in the experiments. This differentiation was made because the difference in ionic mobilities is considered to be the main factor causing asymmetric distribution of the static (intensity of luminescence) and dynamic (velocity of convection) properties of the observed patterns.[8]

4. Results

Figures 5−7 represent the results of the simulations after different time intervals of (a) the concentration profiles of the ions of rubrene and the supporting electrolyte, (b) the electric potential gradient, the associated excess charge density, and the product of these two quantities representing the driving force density for convection. The diffusion coefficients were set equal in this case, hence the symmetric distributions across the interelectrode distance d. The three sets of data cover the time interval from the early stage of the evolution of transport processes (10 ms) up to the stage when recombination and luminescence become visible (60 ms).

Integration over half the interelectrode distance yields the following driving forces for convection (per unit area): 2.5×10^{-6} N cm^{-2} after 10 ms and 3.0×10^{-6} N cm^{-2} after 30 ms

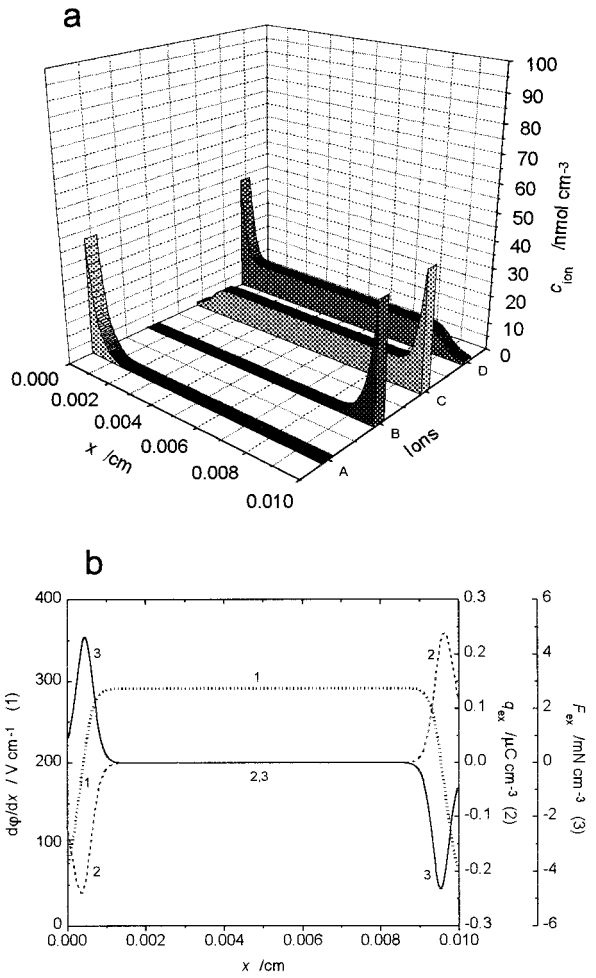

Figure 5. Interelectrode distribution of (a) ions (A) R^-, (B) R^+, (C) An, and (D) Cat and (b) (1) gradient of electric potential, (2) local uncompensated charge q_{ex}, (3) driving force density $F_{ex} = -q_{ex}(\partial\varphi/\partial x)$. Equal diffusion coefficients of all species: 6.2×10^{-6} cm^2 s^{-1} were assumed. Time $t = 10$ ms after beginning of the electrolysis, current $I = 0.135$ mA, solution resistance $R = 20.19$ kΩ.

(with opposite signs for cathode and anode region). For 60 ms the fluxes of rubrene radicals overlap, and recombination takes place in the center of the cell. As can be seen from curve 3 in Figure 7b, there a strong gradient of electric potential develops within a narrow region giving rise to pronounced electric forces. The associated concentration profiles of all species, as depicted in Figure 8a, reflect this effect of recombination by a local increase of the concentration of neutral rubrene molecules (curve E) and simultaneous local decrease of the concentration of all ionic species. Additional simulations showed that this layer of the solution depleted from ions expands as a function of time.

A series of analogous data, but now with a larger diffusion coefficient for the anions of the supporting electrolyte, is reproduced in Figures 9−11 and 8b. Obviously the cathodic region now becomes rapidly depleted from HFP^- ions, and the current in this region is then carried only by rubrene anions and cations of the supporting electrolyte. On the other hand, rubrene cations accumulate in the anodic region. As a consequence the location for recombination of rubrene anions and cations (in the absence of convection) is considerably shifted toward the anode, as becomes evident from Figure 8b.

Now temporal evolution of the asymmetric distribution of electric field and uncompensated charge takes place. The largest coupled cathodic−anodic driving force density for convection spreads from the cathodic toward anodic region in the solution.

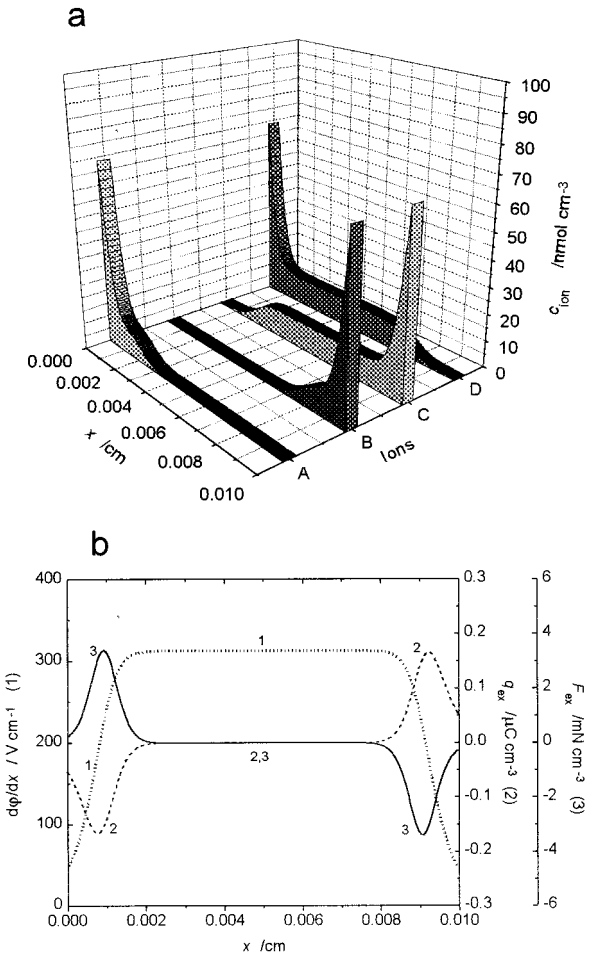

Figure 6. Legend as for Figure 5, for time $t = 30$ ms, current $I = 0.145$ mA, solution resistance $R = 18.65$ kΩ.

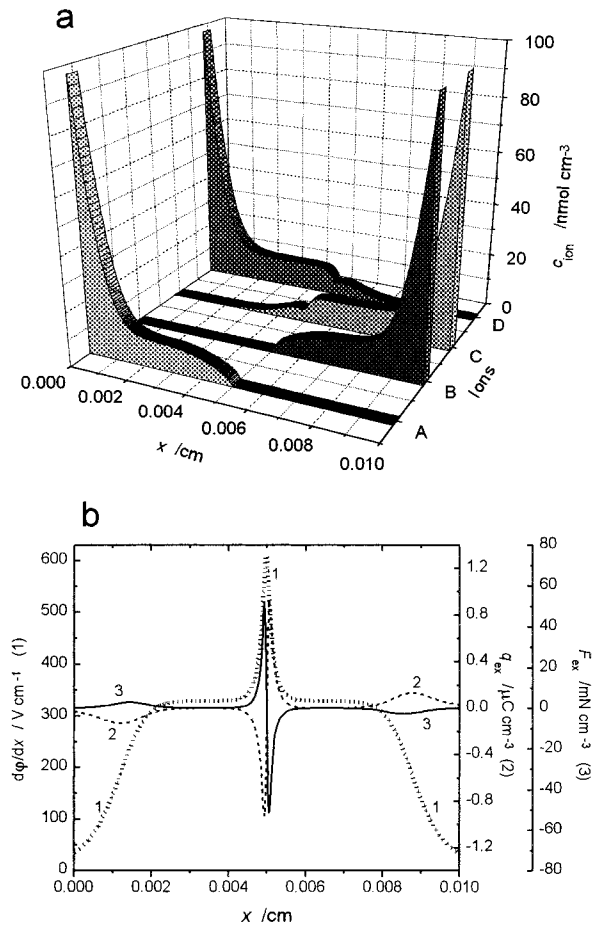

Figure 7. Legend as for Figure 5, for time $t = 60$ ms, current $I = 0.153$ mA, solution resistance $R = 17.54$ kΩ.

The electrical force, persisting close to the anode, is now much smaller. One can distinguish three regions (Δd_1, Δd_2, Δd_3) of the interelectrode space, in which separated nonzero forces exist. The following values of force densities, *integrated* over corresponding distances Δd, were determined. For $t = 10$ ms: $\Delta d_1 = 0-0.15d$, $F_{\text{cath,ex}} = 1.98 \times 10^{-2}$ mN cm^{-2}; $\Delta d_2 = (0.15/0.4)d$, $F_{\text{anod,ex}} = -1.90 \times 10^{-2}$ mN cm^{-2}; $\Delta d_3 = (0.4/1.0)d$, $F_{\text{anod,ex}} = -8.9 \times 10^{-4}$ mN cm^{-2}. For $t = 30$ ms: $d_1 = 0-0.4d$, $F_{\text{cath,ex}} = 8.54 \times 10^{-3}$ mN cm^{-2}; $d_2 = (0.4/0.7)d$, $F_{\text{anod,ex}} = -8.17 \times 10^{-3}$ mN cm^{-2}; $\Delta d_3 = (0.7/1.0)d$, $F_{\text{anod,ex}} = -4.0 \times 10^{-4}$ mN cm^{-2}. As can be seen, at a given time the total driving forces for the directions toward the anode and the cathode are about equal, but considerably (three to eight times) larger than for the previous case with equal diffusion coefficients for all species.

5. Discussion

Schaper and Schnedler[7] had previously proposed a numerical model to account for the origin of the observed patterns of chemiluminescence, which was based on the following assumptions: (i) after applying the voltage the region between the electrodes becomes largely depleted from ions that accumulate at the electrodes, (ii) the reduction of rubrene to anions causes the formation of an uncompensated charge in the solution that interacts with the external electric field thus creating the driving force for convection. This model is based on the assumption of essential unipolar charge injection whose mechanism could be ruled out in our previous work.[8] Instead it was demonstrated that a certain concentration of supporting electrolyte is needed and that in fact bipolar charge injection is taking place. This concept was the starting point for the model presented here in which the field distribution and the associated uncompensated charge were evaluated under the assumption that charge is symmetrically injected at both electrodes and that current flow through the solution comprises all ionic species.

For equal diffusion coefficients of all components, the field distribution and driving force for convection is created symmetrically near both electrodes, and as a consequence with the onset of electrolysis a large part of the fluid is forced into motion.

If the mobility of the anions of the supporting electrolyte exceeds the values of the other species (cf. Figures 9−11), as is the case with the experimentally studied system, the propagation of the pronounced field gradient from the cathode toward the anode reflects the progress of a wave of local ohmic resistance, which is enhanced in regions depleted from rapidly moving anions. In this case a gradual acceleration, starting from the cathodic region, of the fluid takes place.

In this case the space between the electrodes is filled more rapidly by rubrene anions than by cations (cf. Figure 8b, 9−11), and the recombination associated with luminescence is expected to take place near the anode. However, experimentally just the opposite observation is made; namely, luminescence is found to be dominant close to the cathode. This effect demonstrates the limitations of the present model, which was intended to provide just a one-dimensional modeling of the conditions leading to the onset of electrochemiluminescence without taking into account the influence of the resulting convective flow on

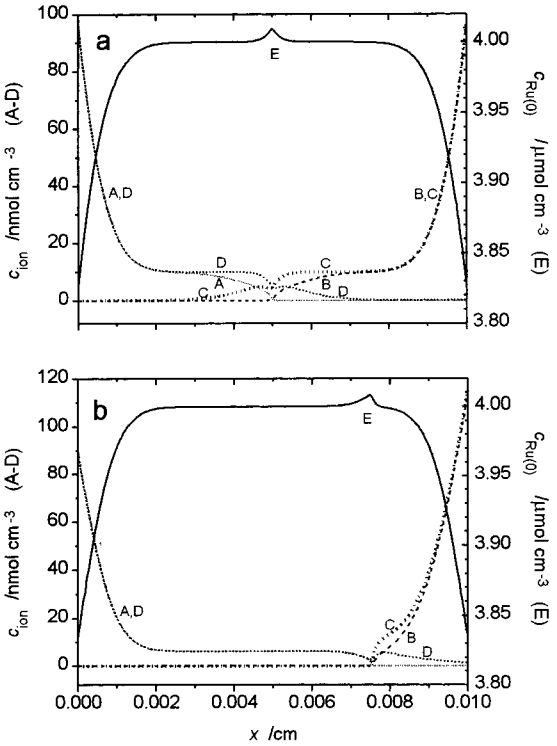

Figure 8. Comparison of concentration profiles of all ionic species (A−D) and rubrene molecules (E) for conditions when rubrene ion radicals meet and recombine in the diffusion-controlled process: (a) equal diffusion coefficients of all species, time $t = 60$ ms (cf. Figure 7), (b) higher diffusion coefficient of the anion (An) of supporting electrolyte, time $t = 50$ ms (cf. Figure 11).

the actual concentration distributions eventually evolving under steady-state conditions.

The development of concentration profiles as reproduced in Figures 7a, 8, and 11a, *without the operation of convection*, would cause the appearance of a layer with homogeneous luminescence inside the solution. Our experimental observations showed indeed that for small distances between the electrodes ($d \leq$ ca. 60 μm), at first a homogeneous burst of luminescence takes place immediately after applying the voltage, rapidly (i.e., <1 s) followed by the formation of stable convective luminescent patterns. On the other hand, such homogeneous luminescence is not observed to precede the appearance of convective structures for larger interelectrode distances where the formation of excess charge and hence of convective flows occurs faster than the interaction between the rubrene ions merely by migration.

The recombination of rubrene radicals is important also for the local conductivity and thus for the distribution of the electric field in the solution. This has the following consequences:

(i) as the simulations show, *in the absence of convection*, recombination of radicals in counterstreams would lead to the formation of an expanding layer of solution largely depleted from all ions. Thus, this region would gain an increasing ohmic resistance, and consequently, the total current should asymptotically tend to zero. On the other hand, in regions closer to the respective electrodes, relatively low-ohmic, concentrated solutions of $\{R^-, TBA^+\}$ and $\{R^+, HFP^-\}$ species would form, for the periods of the order of a few minutes, corresponding to the lifetime of rubrene radicals. However, spontaneously developing convection prevents this distribution by mixing the cathodic and anodic parts of the solution, with simultaneous emission of electrochemiluminescence in the form of patterns, determined by the geometrical distribution of convective flows;

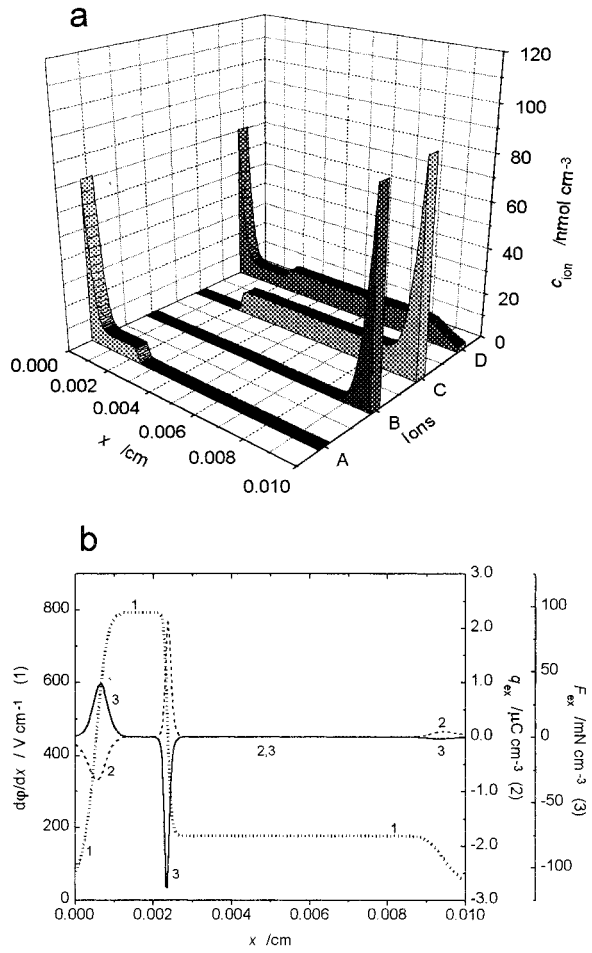

Figure 9. Interelectrode distribution of (a) ions (A) R^-, (B) R^+, (C) An, and (D) Cat and (b) (1) gradient of electric potential, (2) local uncompensated charge q_{ex}, (3) driving force density $F_{ex} = -q_{ex}(\partial\varphi/\partial x)$. Equal diffusion coefficients of rubrene species and cations of supporting electrolyte, 6.2×10^{-6} cm^2 s^{-1} and a higher diffusion coefficient for anions of supporting electrolyte, $D_{An} = 2.8 \times 10^{-5}$ cm^2 s^{-1} were assumed. Time $t = 10$ ms, current $I = 0.226$ mA, solution resistance $R = 11.96$ kΩ.

(ii) since a large nonlinearly distributed gradient of the electric potential develops across the layer in which rubrene radicals recombine, remarkable local driving forces for convection develop there that can induce an intense *local* motion. From our experiments it follows that one of the *most striking* dynamical features of the convective patterns is the complex structure of single luminescent streams (cf. Figure 1), which look like they are composed of many splitted substreams.

6. Conclusions

Starting from a previous report[8] on the formation of chemiluminescent patterns by recombination of electrochemically generated radical anions and cations of rubrene in a thin-layer electrolytic cell, a one-dimensional model was developed for the diffusion and migration processes of neutral and ionic species (including the supporting electrolyte being present with low concentration), which accounts for the *onset* of low-voltage electrohydrodynamic convection. The driving force density for the convection is evaluated from the distribution of the electric field, resulting with the charge injected symmetrically at both electrodes and conducted by the actual local ionic distribution. It is concluded that the observed asymmetric distributions of luminescence across the interelectrode distance are due to differing mobilities of the ions of supporting electrolyte, while

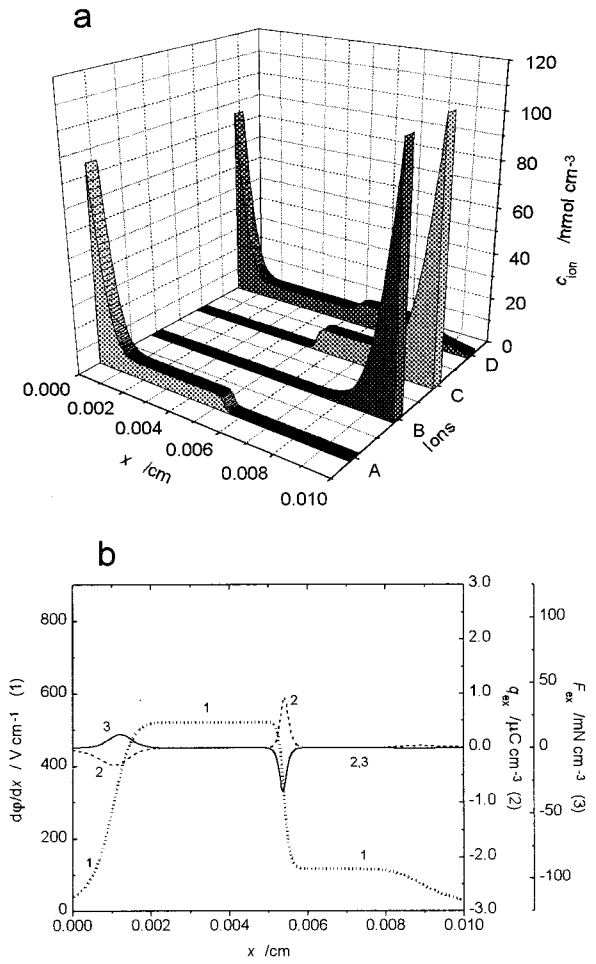

Figure 10. Legend as for Figure 9, for time $t = 30$ ms, current $I = 0.148$ mA, solution resistance $R = 18.19$ kΩ.

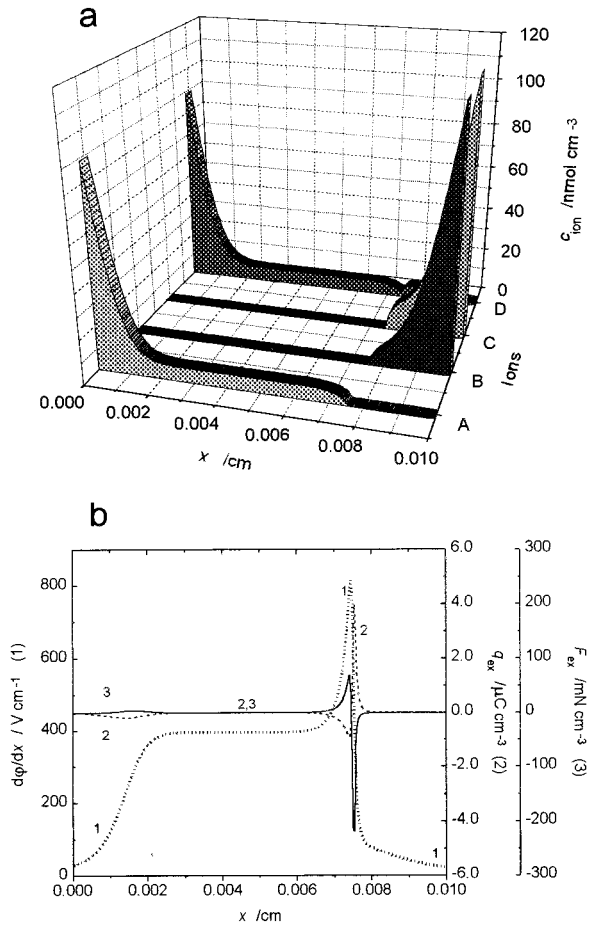

Figure 11. Legend as for Figure 9, for time $t = 50$ ms, current $I = 0.113$ mA, solution resistance $R = 23.91$ kΩ.

creating of rubrene cations and anions occurs with equal rates at both electrodes. The recombination of rubrene radicals (causing the luminescent patterns) was found to additionally complicate the evaluation of the electric field distribution in the respective regions of the interelectrode space.

The presented numerical model underlines the need of detailed electrochemical characterization for full understanding of the effects of chemiluminescence in systems of this type. The next step will consist of analysis of the hydrodynamic processes that are then responsible for the actual properties of the patterns.

Acknowledgment. M.O. gratefully acknowledges a fellowship from the A. v. Humboldt Foundation.

References and Notes

(1) Bénard, H. *Rev. Gen. Sci. Pures Appl.* **1900,** *12*, 1261, 1309.

(2) Chandrasekhar, S. *Hydrodynamic and hydromagnetic stability*; Oxford University Press: New York 1961.

(3) Orlik, M. *Oscillating Reactions. Order and Chaos*; WNT: Warsaw, 1996 (in Polish).

(4) Köstlin, H.; Schaper, H. *Phys. Lett.* **1980**, *76A*, 455.

(5) Schaper, H.; Köstlin, H.; Schnedler, E. *J. Electrochem. Soc.* **1982**, *129*, 1289.

(6) Schaper, H.; Schnedler, E. *J. Phys. Chem.*, **1982**, *86*, 4380.

(7) Schaper, H.; Schnedler, E. *J. Electroanal. Chem.* **1982**, *137*, 39.

(8) Orlik, M.; Rosenmund, J.; Doblhofer, K.; Ertl, G. *J. Phys. Chem. B* **1998**, *102*, 1397.

(9) Laser, D.; Bard, A. J. *J. Electrochem. Soc.* **1976**, *123*, 1834.

(10) Jaworski, A.; Donten, M.; Stojek, Z. *J. Electroanal. Chem.*, **1996**, *407*, 75.

(11) Riddick, J. A., Bunger W. B., Sakano T. K., Eds. *Techniques of Chemistry. Vol. II (Organic Solvents)*, 4th ed.; Wiley: New York, 1986; p 296.

(12) Feldberg, S. W., in Bard, A. J., Ed. *Electroanalytical Chemistry*; Marcel Dekker: New York, 1986; Vol. 3, p 199.

(13) Britz, D. *Digital Simulation in Electrochemistry*, 2nd ed.; Springer: Berlin, 1988.

(14) Bard, A. J.; Faulkner, L. R. *Electrochemical Methods*; Wiley: New York, 1980 and references therein.

(15) Lavagnini, I.; Magno, F. *Anal. Chim. Acta* **1988**, *211*, 75.

(16) Kapturkiewicz, A. *J. Electroanal. Chem.* **1994**, *372*, 101.